Send Orders for Reprints to reprints@benthamscience.ae

Open Access

Dependence of the Deformation of 128×128 InSb Focal-plane Arrays on the Silicon Readout Integrated Circuit Thickness

Xiaoling Zhang[1], Qingduan Meng[2,*] and Liwen Zhang[2]

[1] *School of Information Engineering, Henan University of Science and Technology, Luoyang 471023, China*

[2]*School of Electrical Engineering, Henan University of Science and Technology, Luoyang 471023, China*

Abstract: The square checkerboard buckling deformation appearing in indium antimonide infrared focal-plane arrays (InSb IRFPAs) subjected to the thermal shock tests, results in the fracturing of the InSb chip, which restricts its final yield. In light of the proposed three-dimensional modeling, we proposed the method of thinning a silicon readout integrated circuit (ROIC) to level the uneven top surface of InSb IRFPAs. Simulation results show that when the silicon ROIC is thinned from 300 μm to 20 μm, the maximal displacement in the InSb IRFPAs linearly decreases from 7.115 μm to 0.670 μm in the upward direction, and also decreases linearly from 14.013 μm to 1.612 μm in the downward direction. Once the thickness of the silicon ROIC is less than 50 μm, the square checkerboard buckling deformation distribution presenting in the thicker InSb IRFPAs disappears, and the top surface of the InSb IRFPAs becomes flat. All these findings imply that the thickness of the silicon ROIC determines the degree of deformation in the InSb IRFPAs under a thermal shock test, that the method of thinning a silicon ROIC is suitable for decreasing the fracture probability of the InSb chip, and that this approach improves the reliability of InSb IRFPAs.

Keywords: Crack, infrared focal plane arrays, modeling.

1. INTRODUCTION

Indium antimonide infrared focal-plane arrays (InSb IRFPAs) are a critical component in many of the military and civilian applications for the 3 μm to 5 μm spectral range [1, 2]. To obtain a high signal-to-noise ratio, InSb IRFPAs are usually operated at liquid nitrogen temperature (77 K). Once the thermal mismatch strain accumulated in the InSb chip is larger than its fracture strength, cracks appear in the InSb chip, which limits the final yield of InSb IRFPAs [3]. To improve the reliability of InSb IRFPAs, the InSb chip is usually thinned to a thickness of less than 10 μm to accommodate the thermal mismatch between the InSb chip and the silicon ROIC. Furthermore, both an aluminium nitride (AlN) motherboard and an Invar36 pedestal with a thicknesses greater than 6 millimeters are also chosen for their thermal compatibility with the silicon ROIC [3]. In HgCdTe IRFPAs, a balanced composite structure is employed to prevent the bending of the HgCdTe IRFPAs, which is situated beneath the silicon ROIC [4]. None of these reported successful cases provide answers to certain questions, such as: 1) Where does the thermal strain start? 2) What is the transferring rule of the thermal strain in the layered structure? 3) How can the degree of deformation be decreased? In our previous research [5], we found that the global square checkerboard buckling pattern, which appears in the top surface of the InSb IRFPAs, originates from the thermal mismatch between the silicon ROIC and the intermediate layer above. When passing through both the intermediate layer and the InSb chip, the deformation amplitude is attenuated. In this paper, thinning the silicon ROIC is proposed as a method to further lessen the deformation amplitude in 128×128 InSb IRFPAs, and the dependence of the deformation displacement along the normal direction on the silicon ROIC thickness is obtained. All these ideas help to understand the interactions in the multilayer structure.

2. THREE-DIMENSIONAL MODELING AND PARAMETER SELECTION

InSb IRFPAs are composed of three layers, including the top InSb photosensitive layer, the bottom silicon ROIC, and the intermediate interconnecting layer, consisting of the indium bump array and the reticular underfill. InSb IRFPAs are usually fabricated by flip-chip bonding technology. That is, indium bumps are formed first on both the detector array and the silicon ROIC, then both the detector array and the silicon ROIC are aligned, and a force is applied to cause the indium bumps to cold-weld together. After that, the underfill is dispensed between the InSb die and the silicon ROIC to increase the reliability of the indium bump. The structure of InSb IRFPAs is complex, and they have characteristic sizes ranging from a few micrometers to several centimeters. Many elements are generated in the model meshing process, which causes the stiffness matrix of InSb IRFPAs to be too

*Address correspondence to this author at the School of Electrical Engineering, Henan University of Science and Technology, No. 263, Kaiyuan Road, Luolong District, Luoyang 471023, China; Tel: +86-379-64231157, +86-13525454409; Fax: +86-379-64231910; E-mail: qdmengly@163.com

1874-1290/15 2015 Bentham Open

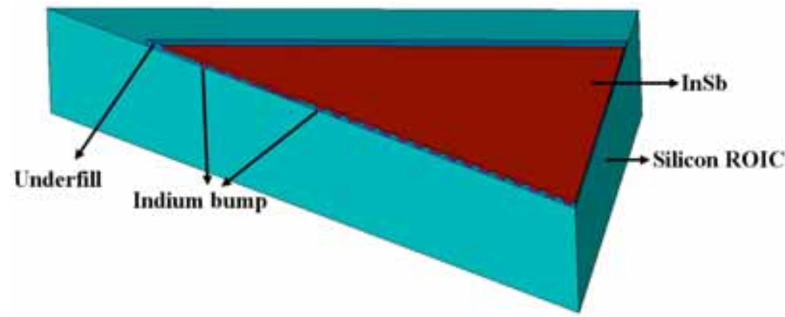

Fig. (1). Three-dimensional modeling of an InSb IRFPAs.

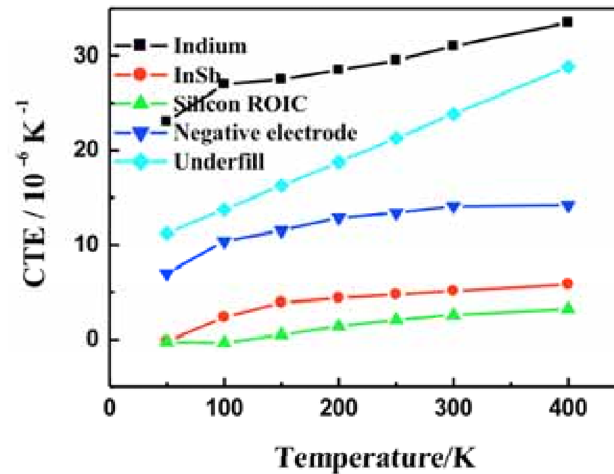

Fig. (2). Coefficients of thermal expansion as a function of temperature for the InSb, indium bump, underfill, negative electrode, and silicon ROIC.

large to be solved. To address this problem, an equivalent modeling was proposed in [6], in which a smaller array is employed to replace the larger array to create a three-dimensional modeling of an InSb IRFPAs, just as shown in Fig. (**1**). In the three-dimensional modeling of the InSb IRFPAs, the InSb chip dimensions are 2500 μm×2500 μm×10 μm, and the chip is attached to the silicon ROIC substrate with a 44×44 indium bump array. The silicon ROIC substrate dimensions are 3200 μm×3200 μm×300 μm. The diameter of each indium bump is 30 μm with a 50 μm pitch. Making use of the geometrical symmetry, here only one-eighth of the overall package is modeled.

The coefficients of thermal expansion (CTEs) of materials depend strongly on the temperature, and usually decrease with decreasing temperature. To calculate the amassed thermal strain in the layered structure, in this paper, the employed CTE models are all temperature-dependent. Both the silicon ROIC and the negative electrode are homogeneous and isotropic linear elastic materials, InSb is an anisotropic linear elastic material [7, 8], and the indium bump is made of a viscoplastic material that has a Young's modulus that increases with decreasing temperature. Once cured, the underfill material is viscoelastic near its glass transition but has an apparent linear elastic behavior at temperatures well below its glass transition temperature. The CTEs for different materials are plotted in Fig. (**2**) [9-14].

3. SIMULATION RESULTS AND DISCUSSION

3.1. Comparison of the Simulated Distribution of the Z-Components of Strain and the Fracture Photograph in InSb IRFPAs

The simulated distribution of the Z-components of strain is shown in Fig. (**3a**); here the maximal Z-components of strain and the minimal Z-components of strain are denoted by MX and MN, respectively. Clearly the maximum Z-components of strain locate in the sites over the negative electrode, and its local extrema present a non-continuous distribution. These agree very well with the fracture features in the fracture photographs of the 128×128 InSb IRFPAs, especially the crack distribution and the locations of the crack initiation sites. Furthermore, in the typical InSb IRFPAs fracture photograph shown in Fig. (**3b**), where the InSb chip touches the indium bump array, it is convex upwards, and where it touches the underfill, it is concave downwards; these characteristics are distinctly displayed in the simulation of the Z-components of strain. The simulated distribution of the Z-components of strain contains all the typical fracture features. Hence the criterion for choosing the Z-components of strain is employed to analyze the thermal deformation of InSb IRFPAs.

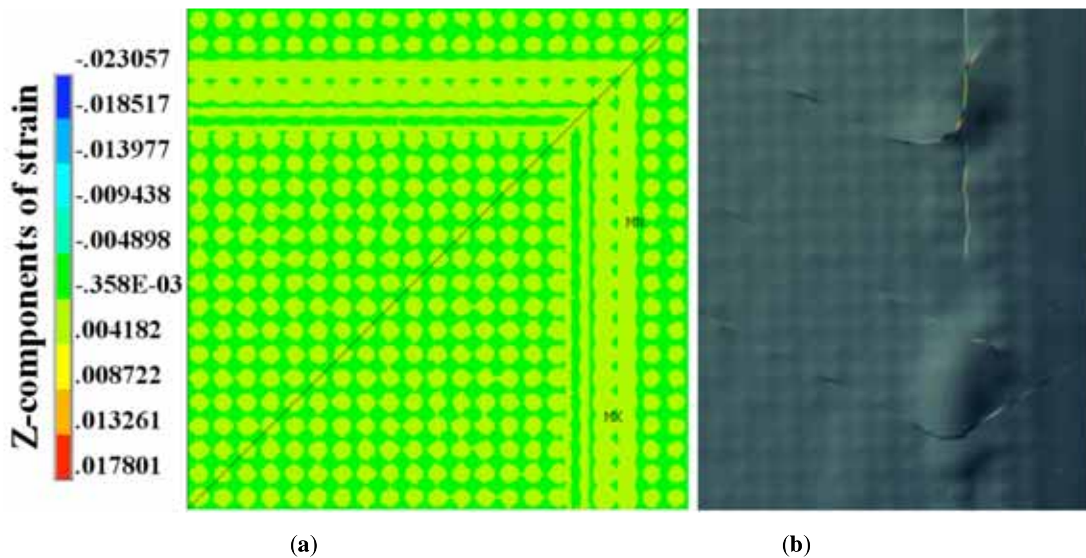

(a) (b)

Fig. (3). Comparison of the simulated and measured deformation distributions on the top surface of InSb IRFPAs: (**a**) simulated Z-components of strain and (**b**) typical fracture photograph.

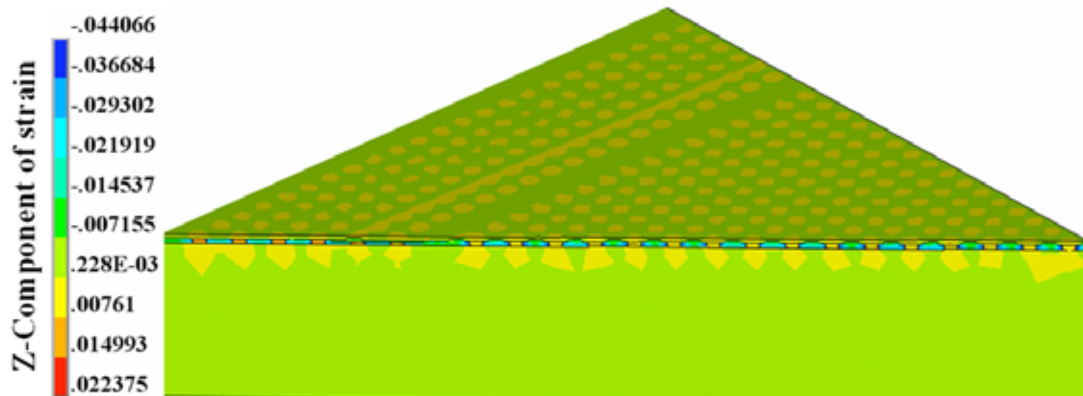

Fig. (4). Distribution of the Z-components of strain along a diagonal cross-section of an InSb IRFPAs.

3.2. Analysis of the Distribution of the Z-components of Strain in the Diagonal Cross-section of InSb IRFPAs

We noticed that on the bottom surface of the silicon ROIC, the Z-components of strain are zero, while on its top surface, the maximal Z-components of strain appear. This indicates that the interactions between the silicon ROIC and the upper layer has a shallow interaction depth and that the interaction depth does not reach the bottom surface of the silicon ROIC. These findings are verified by the distribution of the Z-components of strain in the diagonal cross-section of an InSb IRFPA, as shown in Fig. (**4**). In the silicon ROIC, beneath the indium bump array, the Z-components of strain are clearly larger than those in its surrounding counterparts, and the interaction depth is approximately 42 μm, about 14 percent of the silicon ROIC thickness. Beyond the interaction depth, there are no strain appearing in the silicon ROIC. Thus, the method of thinning the silicon ROIC is proposed to achieve a new equilibrium state with smaller Z-components of strain in InSb IRFPAs.

Usually the flexural rigidity of the thin plate (D) is defined as;

$$D = \frac{Eh^3}{12(1-\nu^2)} \tag{1}$$

where E, ν, and h are the Young's modulus, Poisson's ratio, and thickness of the thin plate, respectively. According to Eq. (1), once the thickness of the silicon ROIC is reduced, its flexural rigidity will decrease sharply, which may help to flatten the top surface of InSb IRFPAs. This assumption is verified by the distribution of the Z-components of strain in the InSb IRFPAs with a thinner silicon ROIC, as shown in Fig. (**5**); here the thickness of the silicon ROIC is set to be 20 μm. Clearly, the thermal strain is redistributed uniformly on the top surface of the InSb IRFPAs, and the square checkerboard buckling deformation distribution disappears. In addition, we learned that the thinned silicon ROIC design was employed in HgCdTe IRFPAs assemblies with a balanced composite structure [15], where the silicon ROIC thickness is reduced to less than 40 μm to allow continued detector performance after a test involving over 1000 thermal cycles (300 K–80 K). All of these findings prove that the method of thinning the silicon ROIC is suitable for reducing the

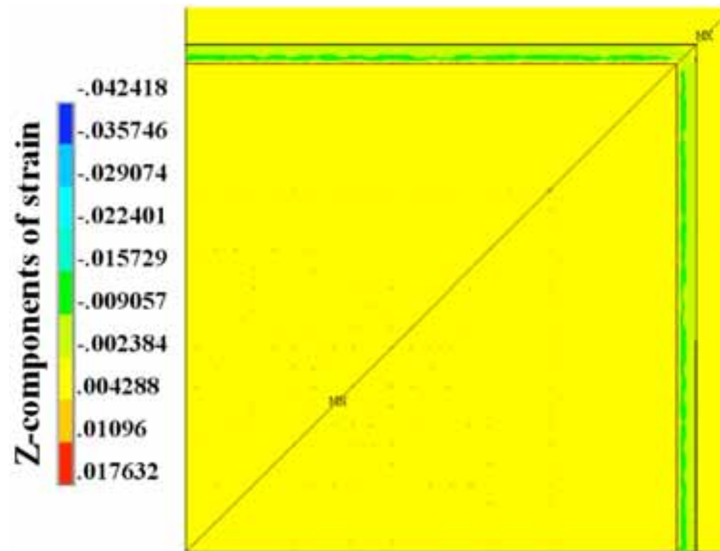

Fig. (5). Simulated Z-components of strain of an InSb IRFPAs with a 20-µm-thick silicon ROIC.

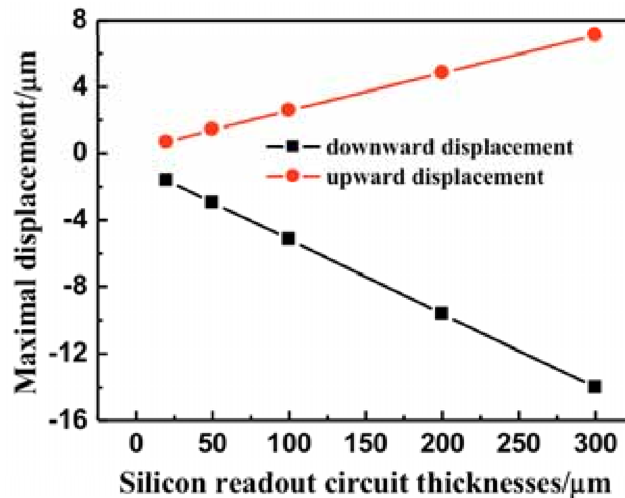

Fig. (6). Maximal Z-components of the displacement in the InSb IRFPAs for different values of the silicon ROIC thickness.

deformation amplitude in InSb IRFPAs under a thermal shock test.

3.3. Silicon ROIC Thickness Dependence of the Deformation of 128×128 InSb IRFPAs

To explore the effect of the silicon ROIC thickness on the Z-components of the displacement of the InSb IRFPAs, here the silicon ROIC thickness is reduced from 300 µm to 20 µm, and all other structural dimensions are kept unchanged. The simulated Z-components of the displacement are shown in Fig. (**6**), where the positive displacement represents upward deformation and the negative displacement represents downward deformation.

In Fig. (**6**), the maximal displacements in the normal direction are plotted for various silicon ROIC thicknesses. When the thickness of the silicon ROIC is thinned from 300 µm to 20 µm, its maximal upward displacement almost decreases linearly from 7.115 µm to 0.670 µm; at the same time, its maximal downward displacement also decreases linearly from 14.013 µm to 1.612 µm. These linear relationships are represented by the formulas;

$$D_u = 0.2617 + 0.0229 \times H \tag{2}$$

$$D_d = -0.7323 - 0.0443 \times H \tag{3}$$

where D_u and D_d are the maximal upward displacement and maximal downward displacement appearing in the InSb IRFPAs, respectively, and H is the thickness of the silicon ROIC. Apparently, in the InSb IRFPAs with a thinner silicon ROIC, both the maximal upward displacement and the maximal downward displacement become smaller, and the rate of the downward displacement change is twice as large as the rate of the upward displacement change. Thus it is deduced that thinning the silicon ROIC is an efficient method for decreasing the deformation amplitude of InSb IRFPAs.

CONCLUSION

Employing a three-dimensional modeling of InSb IRFPAs, we obtained the distribution of the Z-components of strain in the top surface of InSb IRFPAs, which is almost identical with the typical fracture photograph of InSb IRFPAs, especially in terms of the crack initiation sites, the crack distribution, and the global square checkerboard buckling pattern that present on the top surface of InSb IRPFAs. Thus the criterion for choosing the Z-components of strain is employed to analyze the thermal deformation of InSb IRFPAs. We noticed that the interaction depth between the silicon ROIC and the upper layers did not reach the bottom surface of the silicon ROIC, thus the method of thinning the silicon ROIC is proposed to level the uneven top surface of InSb IRFPAs under the thermal shock test. Our analytical results show that the maximal deformation amplitude in the InSb IRFPAs is proportional to the thickness of the silicon ROIC, and the method of thinning the silicon ROIC is suitable for decreasing the fracture probability of the InSb chip.

CONFLICT OF INTEREST

The authors confirm that this article content has no conflict of interest.

ACKNOWLEDGMENTS

The research was supported by the Young Scientists Fund of the National Natural Science Foundation of China (Grant No. 61107083 and 61205090) and by the Aero Science Foundation of China (Grant No. 20100142003).

REFERENCES

[1] Y.T. Gau, L.K. Dai, S.P. Yang, P.K. Weng, K.S. Huang, Y.N. Liu, C.D. Chiang, F.W. Jih, Y.T. Cherng, and H. Chang, "256×256 InSb Focal Plane Arrays", In: *Proc. SPIE: Optoelectronic Materials and Devices II*, 2000, pp. 467-479.

[2] W. Parrish, J. Blackwell, G. Kincaid, and R. Paulson, "Low-cost high performance InSb 256×256 infrared camera", In: *Proc. SPIE: Infrared Technology XVII*, 1991, pp. 274-284.

[3] K.M. Merrill, A. Fowler, W. Ball, A. Henden, F. Vrba, and C. McCreight, "Orion II: the second generation readout multiplexer for the largest infrared hybrid focal plane", In: *Proc. SPIE: Focal Plane Arrays for Space Telescopes*, 2004, pp. 186-193.

[4] G. Finger, R.J. Dorn, M. Meyer, L. Mehrgan, J. Stegmeier, and A. Moorwood, "Hybrid active pixel sensors in infrared astronomy", *Nucl. Instrum. Meth. Phys. Res. A*, vol. 549, pp. 79-86, 2005.

[5] X.L. Zhang, Q.D. Meng, Q. Yu, L.W. Zhang, and Y.Q. Lv, "Thermal buckling analysis in InSb focal plane array detector", *J. Mech. Sci. Technol.*, vol. 27, pp. 1809-1813, 2013.

[6] Q.D. Meng, X.L. Zhang, L.W. Zhang, and Y.Q. Lv, "Structural modeling of 128 × 128 InSb focal plane array detector", *Acta Phys. Sin.*, vol. 61, pp. 190701-190706, 2012.

[7] Q.D. Meng, Q. Yu, L.W. Zhang, and Y.Q. Lv, "Mechanical parameters selection in InSb focal plane array detector normal direction", *Acta Phys. Sin.*, vol. 61, pp. 226103-226105, 2012.

[8] A. Pandolfi, and K. Weinberg, "A numerical approach to the analysis of failure modes in anisotropic plates ", *Eng. Fract. Mech.*, vol. 78, pp. 2052-2069, 2011.

[9] Y. He, B.E. Moreira, A. Overson, S.H. Nakamura, C. Bider, and J.F. Briscoe, "Thermal characterization of an epoxy-based underfill material for flip chip packaging", *Thermochim Acta*, vol. 357-358, pp. 1-8, 2000.

[10] G.K. White, and J.G. Collins, "Thermal expansion of copper, silver, and gold at low temperatures", *J. Low. Temp. Phys.*, vol. **7**, pp. 43-75, 1972.

[11] X. Cheng, C. Liu, and V.V. Silberschmidt, "Numerical analysis of thermo-mechanical behavior of indium microjoint at cryogenic temperatures", *Comp. Mater. Sci.*, vol. 52, pp. 274-281, 2012.

[12] R.W. Chang, and M.F. Patrick, "Constitutive relations of indium in extreme temperature electronic packaging based on Anand model", *J. Electron. Mater.*, vol. 38, pp. 1855-1859, 2009.

[13] D.F. Gibbons, "Thermal expansion of some crystals with the diamond structure", *Phys. Rev.*, vol. 112, pp. 136-140, October 1958.

[14] Y. Okada and Y. Tokumaru, "Precise determination of lattice parameter and thermal expansion coefficient of silicon between 300 and 1500 K", *J. Appl. Phys.*, vol. 56, pp. 314-320, 1984.

[15] T. Kanno, H. Wada, M. Nagashima, H. Wakayama, K. Awamoto, N. Kajihara, Y. Ito, and M. Nakamura, "256×256 element HgCdTe hybrid IRFPA for 8- to 10-μm band", In: *Proc. SPIE: Infrared Technology XXI*, 1995, pp. 384-391.

Received: June 09, 2014 Revised: June 22, 2014 Accepted: November 24, 2014

© Zhang *et al.*; Licensee *Bentham Open*.

This is an open access article licensed under the terms of the Creative Commons Attribution Non-Commercial License (http://creativecommons.org/licenses/by-nc/3.0/) which permits unrestricted, non-commercial use, distribution and reproduction in any medium, provided the work is properly cited.